Isobaric yield curves at $A = 72$ from the spallation of medium mass isotopes by intermediate energy protons

Michael J. Tobin
Department of Radiation Health, University of Pittsburgh, Pittsburgh, Pennsylvania 15261

Paul J. Karol
Department of Chemistry, Carnegie-Mellon University, Pittsburgh, Pennsylvania 15213
(Received 27 October 1988)

Cross sections of radionuclides in the $A \approx 72$ mass region produced by the interaction 800 MeV protons with ^{89}Y, ^{92,96,100}Mo, and ^{130}Te were measured. Particular emphasis was paid to the measurement of short-lived products far from β stability. The cross sections were used to generate isobaric yield curves at $A = 72$. Precise characterization of these curves showed that the distribution parameters (mean, standard deviation, skewness) vary in a regular fashion with target N/Z. For ^{89}Y, relative isobaric curves produced by 500 and 800 MeV protons were found to be identical within experimental error. The yield distributions for the ^{92,96,100}Mo targets also scaled with those from an earlier alpha-induced spallation study. These findings lend strong support to the argument that the spallation mechanism is independent of projectile energy and target composition.

I. INTRODUCTION

Many studies of the interaction of intermediate and high-energy hadrons with complex target nuclei have been well described in terms of the two-step spallation model proposed by Serber.[1] Indeed, they have been labeled an "undisputed tacit assumption" by Hüfner[2] in his recent review.

In the first step of the reaction model, projectile-target interactions occur via individual nucleon-nucleon collision. These propagate an intranuclear cascade leading to the prompt emission of nucleons and light fragments. Excitation energy and forward momentum are imparted to the residual nucleus. With relativistic heavy-ion projectiles, this process is referred to as abrasion. In the slower, second step of the reaction, excitation energy is dissipated via the evaporation of nucleons and light nuclei. Over the years, this sequence has been known as the "cascade-evaporation" model. In more recent heavy-ion studies, the analogous "abrasion-ablation" model is invoked.

The spallation process has been characterized by the study of isobaric yield distributions from different target and/or projectile systems.[3] The isobaric yield curve shows the dependence of formation cross section upon nuclear charge (hence stability) for a given mass number. In addition to providing information on the reaction mechanism, knowledge of yield systematics is pertinent to isotope production fields[4] such as cosmochemistry, nuclear medicine, and structure studies of exotic neutron-rich nuclei.

From medium-mass target nuclei, isobaric yield distributions are roughly Gaussian in form, peaking somewhat to the neutron deficient side of stability. Early spallation studies measured the isobaric yields of long-lived, near-stable products.[5,6] From various medium-mass targets, a given isobaric yield distribution from proton-induced reactions seemed to be independent of target mass. Miller and Hudis[7] hypothesized that this apparent universality was a result of the evaporation step washing out any "memory" of the initial target composition. That is, near-stable spallation products arise from a wide variety of cascade-evaporation pathways converging on stability. This insensitivity is still regarded as a characteristic feature of spallation.[3]

However, Monte Carlo simulations predicted that isobaric yield distributions should reflect the composition (N/Z) of the target nucleus: spallation of neutron excess targets should give enhanced yields of neutron excess products and vice versa.[8] Several studies subsequently confirmed the dependence of spallation yield systematics on the composition of the target. Porile and Church[9] measured $A = 72$ isobaric yield distribution from 1.8 GeV protons on ^{96}Ru, ^{96}Mo, and ^{96}Zr and found that the most probable product N/Z increased with increasing target N/Z. Thibault-Phillipe[10] reported similar behavior for Na isotopic distributions from 24 GeV protons on ^{92}Mo and ^{100}Mo. Ku and Karol[11] measured $A = 72$ yield distributions from the interaction of 720 MeV alpha particles with ^{92,96,100}Mo targets. In the latter study, an extensive analysis showed that not only the most probable product N/Z, but also the distribution variance varied regularly with target N/Z. In spite of the dominant role of the nuclear mass-energy surface forcing evaporative deexcitation towards stability, these studies showed the distributions in fact retain considerable "memory" of the initial target composition.

Most experts seem to agree that the mechanism of intermediate energy spallation (but not fragmentation) has been by and large determined.[2] However, the majority of studies supporting the Serber model have surveyed the high-yield, longer-lived products close to β stability, whose many possible formation pathways provide only averaged information. In contrast, products far from β

stability arise from a restricted pool of cascade-evaporation pathways. This realization was the motivation behind the present investigation: to try to resolve the two reaction steps by more meaningful focus on shorter-lived species on the outlying wings of the charge dispersion curve.

One of the principal objectives of this study was to measure the shape of the yield distributions resulting from proton-induced spallation for comparison with the 720-MeV alpha results of Ku and Karol. Fourteen Ge and As yields from the interaction of 800-MeV protons with ^{92}Mo, ^{96}Mo, ^{100}Mo, and ^{89}Y were obtained. Germanium and arsenic were selected for study for several reasons. First, the isotopic distributions span a wide N/Z range (^{66}Ge $N/Z \approx 1.06$ to ^{79}As $N/Z \approx 1.4$) about mass 72. Second, their chemical properties lend themselves to rapid chemical separations with reasonably high yields facilitating measurement of the low-cross-section, short-lived activities. In addition, the cross sections of 16 gallium and bromine isotopes from the interaction of 800 MeV protons with ^{89}Y were determined as part of an ancillary integral recoil study.[12] Yields were corrected according to established mass-yield systematics to generate an "$A=72$" isobaric distribution.

The *relative* yields of As and Ge products from the interaction of 500 MeV protons with ^{89}Y were also measured. Comparison of the resultant isobaric yield distribution shapes to those measured at 800 MeV tests Miller and Hudis' hypothesis of the projectile energy independence of spallation yield systematics (aside from scaling).[7]

The nearly linear behavior of the most probable product N/Z (at $A=72$) with target composition was found by Ku and Karol to extend smoothly to the heavy target ^{197}Au. To verify that this extrapolation is proper and not due to a contribution from high-energy fission, the very neutron-rich target ^{130}Te was studied.

TABLE I. Decay properties of nuclides studied (Refs. 14 and 15).

Nuclide	Half-life	Measured γ (keV)	Abundance
^{65}Ga	15.2 min	115.1	0.58
^{66}Ga	9.4 h	1039.4	0.38
^{67}Ga	78.3 h	93.3	0.48
^{68}Ga	68.1 min	1077.5	0.03
^{70}Ga	21.1 min	1039.6	0.067
^{72}Ga	14.1 h	833.9	0.956
^{73}Ga	4.86 h	297.0	0.80
^{74}Ga	8.25 min	596.0	0.912
^{66}Ge	2.27 h	381.8	0.28
^{67}Ge	19.0 min	167.0	0.774
^{69}Ge	39.0 h	1106.4	0.257
^{75}Ge	82.8 min	264.8	0.111
^{77}Ge^{g}	11.3 h	264.8	0.533
^{78}Ge	1.45 h	277.3	0.96
^{69}As	15.2 min	233.0	0.05
^{70}As	52.5 min	1039.6	0.817
^{71}As	64.8 h	174.9	0.836
^{72}As	26.0 h	834.0	0.801
^{74}As	17.8 d	595.8	0.603
^{76}As	26.3 h	559.1	0.45
^{78}As	90.6 min	614.0	0.54
^{79}As	9.01 min	95.5	0.165
^{73}Br	3.4 min	64.9	0.34
^{74}Br^{m}	41.5 min	635.0	0.98
^{74}Br^{g}	25.3 min	635.0	0.98
^{75}Br	95.5 min	286.5	0.916
^{76}Br	16.1 h	559.0	0.74
^{77}Br^{m}	4.28 min	106.0	0.137
^{77}Br^{g}	57.04 h	239.0	0.228
^{78}Br	6.46 min	614.0	0.136
^{80}Br^{m}	4.42 h	616.0	a
^{80}Br^{g}	17.68 min	616.0	0.067
^{82}Br^{g}	35.34 h	776.0	0.83

[a]Determined through ^{80}Br^{g} daughter.

II. EXPERIMENTAL

To facilitate the rapid chemical separations, water soluble salts of the enriched ($\geq 96\%$) ^{92}Mo, ^{96}Mo, ^{100}Mo, ^{130}Te, and high purity ($\geq 99.9\%$) ^{89}Y target metals were synthesized or purchased. Self-supporting 1.50×2.00 cm target pellets were prepared using a hydraulic press. Effective target thickness was 10–50 mg/cm^2 enriched metal. For absolute yield determinations, targets were placed in individual stacks with 25 μm aluminum catcher and monitor foils. The target stacks were carefully aligned and sealed in 100 μm aluminum envelopes.

All irradiations were performed at Los Alamos National Laboratory using the LAMPF 800 MeV external proton beam. Irradiation times were 1–5 min with a beam intensity of 1–5 μA. Targets were delivered to the nuclear chemistry lab via a pneumatic rabbit system.

Since the spallation products of interest have low formation cross sections and short half-lives, rapid and reasonably quantitative chemical separations were essential. Solvent extraction and ion exchange separations were used involving trace (≤ 500 μg) amounts of carrier, reducing equilibration times and volumes without loss of selectivity or efficiency. Separation times were 4–8 min. Chemical yields were determined spectrophotometrically.[13]

Decay properties[14,15] of the observed nuclides are listed in Table I. Counting was performed at LAMPF using calibrated Ge(Li) spectrometers. Product and monitor decay curves were analyzed by a nonlinear least squares program.[16]

III. RESULTS

Absolute cross sections were obtained by normalization to the ^{27}Al$(p,3pn)^{24}$Na monitor reaction taken to be 10.5 ± 0.5 mb.[17] Results from the interaction of 800 MeV protons with ^{89}Y, $^{92-100}$Mo, and ^{130}Te targets are presented in Table II. I, $\sim I$, and C refer, respectively, to independent, effectively independent, or cumulative formation. "Effectively" independent implies that the measured or estimated contribution from precursors is only a small fraction of the observed yield. N/Z, the neutron-to-proton ratio of each product, is given in column 2. The tabulated yields are the arithmetic mean of three replicate determinations. The reported uncertainties reflect the total (random and systematic) experimental error.

TABLE II. 800 MeV proton-induced spallation cross sections (mb).

Nuclide	N/Z	^{89}Y	^{92}Mo	^{96}Mo	^{100}Mo	^{130}Te
^{66}Ge I	1.063	$(9.6\pm0.9)\times10^{-2}$	0.17 ± 0.015	$(4.4\pm0.5)\times10^{-2}$	$(2.3\pm0.4)\times10^{-3}$	$(2.2\pm0.6)\times10^{-4}$
^{67}Ge $\sim I$	1.094	1.9 ± 0.1	1.72 ± 0.12	0.5 ± 0.04	$(9.8\pm0.7)\times10^{-2}$	$(3.5\pm0.6)\times10^{-3}$
^{69}Ge C	1.156	13.3 ± 1.2	8.7 ± 1.0	3.8 ± 0.3	2.2 ± 0.2	0.11 ± 0.018
^{75}Ge C	1.344	$(5.8\pm0.8)\times10^{-2}$	$(8.3\pm1.8)\times10^{-3}$	$(3.9\pm1.0)\times10^{-2}$	$(9.5\pm2.2)\times10^{-2}$	0.15 ± 0.03
^{77}Ge^{g} I	1.406	$(5.3\pm1.5)\times10^{-4}$			$(9.6\pm4.6)\times10^{-3}$	$(5.6\pm1.3)\times10^{-3}$
^{78}Ge $\sim I$	1.438				$(1.1\pm0.63)\times10^{-4}$	$(5.9\times2.3)\times10^{-4}$
^{69}As I	1.091	0.7 ± 0.05	0.87 ± 0.09	0.17 ± 0.02	$(4.0\pm0.6)\times10^{-2}$	$(1.7\pm0.4)\times10^{-3}$
^{70}As C	1.121	1.9 ± 0.1	2.3 ± 0.2	0.39 ± 0.05	0.17 ± 0.02	$(3.9\pm0.9)\times10^{-2}$
^{71}As C	1.152	11.3 ± 0.8	10.6 ± 1.0	5.1 ± 0.4	2.3 ± 0.2	0.10 ± 0.03
^{72}As $\sim I$	1.182	10.4 ± 0.9	9.5 ± 1.1	5.3 ± 0.4	4.2 ± 0.4	0.43 ± 0.08
^{74}As I	1.242	5.7 ± 1.6	1.9 ± 0.4	1.9 ± 0.3	3.2 ± 0.8	1.3 ± 0.2
^{76}As I	1.303	0.5 ± 0.07	0.16 ± 0.04	0.28 ± 0.02	0.8 ± 0.1	0.74 ± 0.12
^{78}As $\sim I$	1.364	$(1.5\pm0.3)\times10^{-2}$		$(1.5\pm0.3)\times10^{-2}$	$(4.6\pm0.8)\times10^{-2}$	$(7.5\pm1.3)\times10^{-2}$
^{79}As $\sim I$	1.394	$(1.8\pm0.4)\times10^{-3}$		$(2.9\pm1.1)\times10^{-3}$	$(1.4\pm0.5)\times10^{-2}$	$(1.8\pm0.6)\times10^{-2}$

Nuclide	N/Z	^{89}Y	Nuclide	N/Z	^{89}Y	Meta/ground ratio
^{65}Ga $\sim I$	1.097	1.2 ± 0.2	^{73}Br $\sim I$	1.085	1.9 ± 0.9	
^{66}Ga $\sim I$	1.129	5.9 ± 0.7	^{74}Br^{m} $\sim I$	1.114	3.9 ± 0.5	1.3 ± 0.3
^{67}Ga C	1.161	9.0 ± 1.0	^{74}Br^{g} $\sim I$	1.114	3.0 ± 0.5	
^{68}Ga $\sim I$	1.194	9.2 ± 1.0	^{75}Br C	1.143	17.7 ± 2.1	
^{70}Ga C	1.258	1.2 ± 0.3	^{76}Br $\sim I$	1.171	26.1 ± 3.8	
^{72}Ga $\sim I$	1.323	1.8 ± 0.3	^{77}Br^{m} $\sim I$	1.200	16.1 ± 2.9	1.8 ± 0.8
^{73}Ga $\sim I$	1.355	$(1.7\pm0.7)\times10^{-2}$	^{77}Br^{g} $\sim I$	1.200	9.2 ± 3.7	
^{74}Ga $\sim I$	1.387	$(2.2\pm0.9)\times10^{-3}$	^{78}Br C	1.229	16.8 ± 3.7	
			^{80}Br^{m} I	1.286	2.2 ± 0.8	0.6 ± 0.2
			^{80}Br^{g} I	1.286	3.7 ± 0.3	
			^{82}Br^{g} I	1.343	0.53 ± 0.08	

The principal sources of random error were from target alignment, chemical yields, decay curve fits, and parent-daughter separation times. The sources of systematic error included corrections for minor isotopic constituents in the targets, detector efficiencies, decay schemes, and summing corrections. Previous spallation studies with similar thickness targets indicated that the contribution from secondary reactions would be insignificant.[11,18]

The relative cross sections of As and Ge isotopes from 500 MeV proton interactions with ^{89}Y are presented in Table III. Ge results were normalized to the ^{72}As internal "monitor" using the ratio of the respective chemical yields. For these relative results, the uncertainties reflect only random sources of error.

Based upon the procedures of Ku and Karol and others,[9,11,19,20] $A=72$ isobaric yield distributions were constructed from ($65\leq A\leq80$) measured cross sections. The mass-yield decreases exponentially with increasing mass loss from the target. Therefore, the measured cross sections were corrected to the $A=72$ curve by a factor $\exp[-m(A-72)]$. For each target, m was estimated by a procedure similar to that in Ref. 11. The final logarithmic mass-yield slopes are presented in Table IV.

An initial estimate of the shape of the isobaric yield distribution was drawn through all of the measured independent yields. The estimated precursor yields were then subtracted from the measured cumulative yields. As in earlier work,[11] the uncertainty of the precursor correction was taken to be 20% of the value of the correction. For products such as ^{67}Ge, ^{78}As, and ^{82}Br^{g} on the outlying "wings" of the distribution, the predicted precursor contribution was negligible. For ^{77}Ge^{g}, the correction

TABLE III. 500 MeV proton-induced spallation cross sections (relative to ^{72}As).

Nuclide	N/Z	^{89}Y relative cross section	Nuclide	N/Z	^{89}Y relative cross section
^{66}Ge I	1.063	$(5.7\pm0.7)\times10^{-3}$	^{69}As I	1.091	0.051 ± 0.0006
^{67}Ge $\sim I$	1.094	0.11 ± 0.01	^{70}As C	1.121	0.13 ± 0.02
^{69}Ge C	1.156	1.1 ± 0.12	^{71}As C	1.152	0.71 ± 0.08
^{75}Ge C	1.344	$(3.7\pm0.6)\times10^{-4}$	^{72}As $\sim I$	1.182	1.0 ± 0.08
^{77}Ge^{g} $\sim I$	1.406	$(7.0\pm2.4)\times10^{-4}$	^{74}As I	1.242	0.41 ± 0.12
			^{76}As I	1.303	$(4.1\pm0.7)\times10^{-2}$
			^{78}As $\sim I$	1.364	$(1.2\pm0.2)\times10^{-3}$
			^{79}As $\sim I$	1.394	$(1.9\pm0.5)\times10^{-4}$

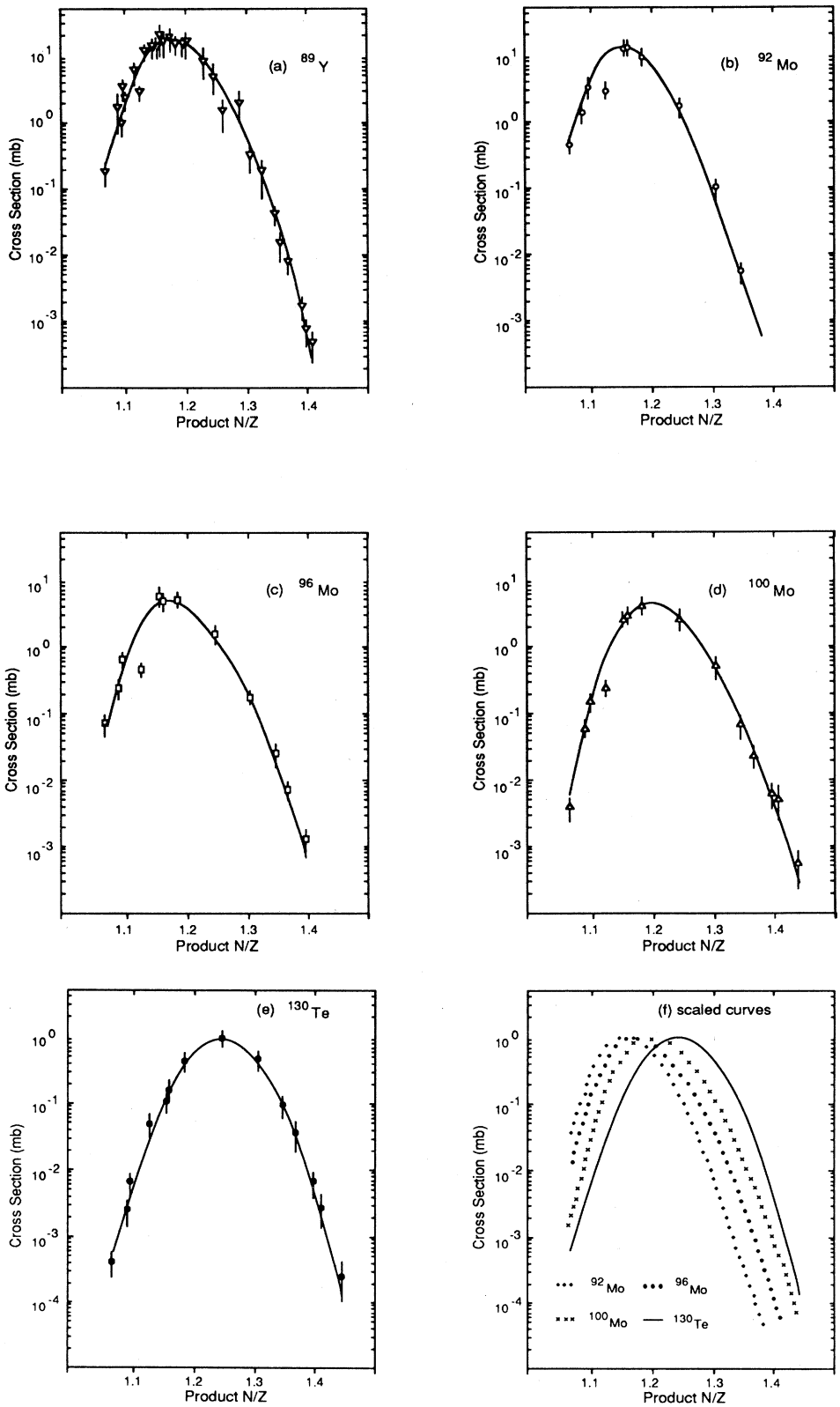

FIG. 1. $A=72$ absolute isobaric yield curves from the interaction of 800 MeV protons with ^{89}Y, ^{92,96,100}Mo, and ^{130}Te targets. Solid curves through data are fits to Eq. (1).

TABLE IV. Logarithmic mass-yield slopes.

Target	500 MeV	800 MeV
^{89}Y	0.138±0.019	0.104±0.011
^{92}Mo		0.113±0.019
^{96}Mo		0.099±0.012
^{100}Mo		0.102±0.011
^{130}Te		0.127±0.016

due to the 80% β^- decay of ^{77}Ge^m was estimated from isomer ratio systematics in a manner similar to that discussed later for ^{70}As. The largest precursor contribution, nearly 12 percent, was that estimated for short-lived ^{71}Se, located near the distribution peak.

Corrected cross sections for the 800 MeV proton irradiations are plotted against N/Z in Figs. 1(a)–(e) for the five targets. The smooth curves represent optimal fits to a skewed distribution function,[21] i.e., a Gaussian modified by the complementary error function

$$Y(X)=\frac{\mu_0'}{2\pi(\mu_2+k^2)^{1/2}}\exp\left[-\frac{(X-\mu_1'-k)^2}{2(\mu_2+k^2)}\right]\mathrm{erfc}(\beta X)\ , \tag{1}$$

where

$$\mu_0'=\sum_{i=0}^{\infty} y_i\Delta X\ , \tag{2}$$

$$\mu_{n>0}'=\frac{\sum_{i=0}^{\infty} x_i^n y_i \Delta x}{\mu_0'}\ , \tag{3}$$

$$\mu_n=\sum_{i=0}^{\infty}(x_i-\mu_1')^n\mu_0'\ , \tag{4}$$

$$k=\left[\frac{2\mu_3}{(4-\pi)}\right]^{1/3}\ , \tag{5}$$

$$\beta=\left\{\frac{\frac{2}{\pi}-\frac{k^2}{(\mu_2+k^2)}}{2\left[\frac{2}{\pi}+\frac{k^2}{(\mu_2+k^2)}\right]}\right\}^{1/2}\ , \tag{6}$$

and erfc is the complementary error function.[22]

Consistent with earlier measurements,[9,10,11,18,19] the following trends are apparent: (1) The location of the distribution maximum shifts towards the neutron excess side of stability with increasing target N/Z. (2) The width of the distribution increases with target N/Z. (3) The distributions are asymmetric, peaking on the neutron deficient side of stability ($N/Z\approx 1.25$) and skewing slightly towards the neutron excess side. With the exception of the distribution from the ^{130}Te target, the neutron deficient "wing" of the isobaric yield curves drops off more rapidly than the neutron excess side.

To better illustrate these observations, the curves are superimposed in Fig. 1(f) and normalized at their peaks. ^{89}Y ($N/Z=1.282$) is indistinguishable from the ^{96}Mo ($N/Z=1.286$) distribution.

IV. DISCUSSION

The targets examined in this study span a wide N/Z range, from ^{92}Mo ($N/Z=1.19$) to ^{130}Te ($N/Z=1.50$). In the conventional two-step spallation model, these differences become obscured during the excitation and relaxation phases of the reaction. For example, from simple combinatorics,[23] one predicts that relatively neutron-rich ^{130}Te would have a higher probability of losing neutrons in the cascade step than relatively neutron poor ^{92}Mo. Thus, the initial N/Z differences of the target nuclei are slightly reduced during the cascade step.

The relaxation process further decreases such differences. In his theoretical treatment of high-temperature nuclei, LeCouteur has shown that the relative likelihood of the evaporation of a charged particle or a neutron from an excited nucleus is strongly dependent upon the location of the cooling nucleus on the nuclear energy surface;[24] particle emission causing the greatest free energy change will be favored. For proton-rich nuclei, charged particle separation energies will be small relative to the neutron separation energies, increasing the probability of charged particle emission. The converse is true for neutron-rich nuclei. As the residual nucleus cools substantially, the Coulomb barrier effectively hinders charged particle evaporation, increasing the likelihood of neutron emission. The net effect of the relaxation stage is initially to channel the cooling nuclei towards the minimum of the nuclear energy surface, "washing out" any initial differences in cascade residual composition and finally to shift slightly to the neutron deficient side of stability.

In spite of the channeling effect, the observed isobaric yield distributions indeed "remember" the composition of the target, as evidenced in Fig. 1(f) by the gradual shift of the distribution peak towards higher N/Z in going from ^{92}Mo to ^{130}Te. The relative widths of the yield curves show a similar increase with target N/Z. Additionally, the slopes on the neutron-deficient side of the curves are uniformly steeper than the neutron-excess side for the Y and Mo targets. This latter effect reflects the role of the nuclear energy surface in preventing extreme excursions from stability. At late stages of the relaxation process, cooling nuclei are already neutron deficient; additional neutron emission is suppressed because of the increasing neutron separation energies as the proton-unstable limit is approached. In contrast, the neutron excess products are relatively far from the neutron-unstable limit because the yield distributions are displaced towards the neutron-deficient side of stability. Since the neutron-excess products from the Y and Mo targets are not strongly influenced by the distant neutron-unstable limit, their relative yields are still quite sensitive to target composition.

The 500 MeV proton-induced relative yields from ^{89}Y and the 720 MeV α-induced spallation absolute cross sections of Ku and Karol[11] (^{92}Mo, ^{96}Mo, and ^{100}Mo targets) were corrected to $A=72$. The resultant isobaric yield curves are compared to the 800 MeV proton-induced re-

sults in Figs. 2(a)–(d). The solid curves are the scaled 800 MeV proton curves. The remarkable congruity in the shape of the isobaric yield distributions from a given target, for both the 500 and 800 MeV proton and 720 MeV alpha projectiles, is strong evidence of the lack of dependence of the spallation mechanism upon the nature of the projectile.

Also shown in Figs. 2(a)–(d) are the product cross section ratios. The 720 MeV α/800 MeV proton ratios are uniform within experimental error across the product N/Z range. In the absence of any mechanistic changes in the spallation process, the α/proton absolute cross section ratios would be expected to reflect the ratio of the total reaction cross sections for the two projectiles. The ratio predicted by the "soft spheres" model[25] for 720 MeV α particles and 800 MeV protons on the $^{92-100}$Mo targets is 1.50. The α/proton ratios are in excellent agreement with the predicted ratio [dashed lines in Figs. 2(b)–(d)].

The fitted distribution shape parameters are listed in Table V and are plotted against target N/Z in Figs. 3(a)–(d). For each target, the parameters are identical, within error. The mean of the $A=72$ isobaric distribution from the interaction of 2.9 GeV protons with ^{197}Au[18] was included in Fig. 3(a) for comparison to the ^{130}Te point. The distribution means from ^{197}Au ($N/Z=1.494$) and ^{130}Te ($N/Z=1.5$) were found to be identical, within the large uncertainty of the Au point, implying that the magnitude of a high-energy fission contribution to the mass 72 products from ^{197}Au is small.

Finally, a noteworthy feature is the anomalously low

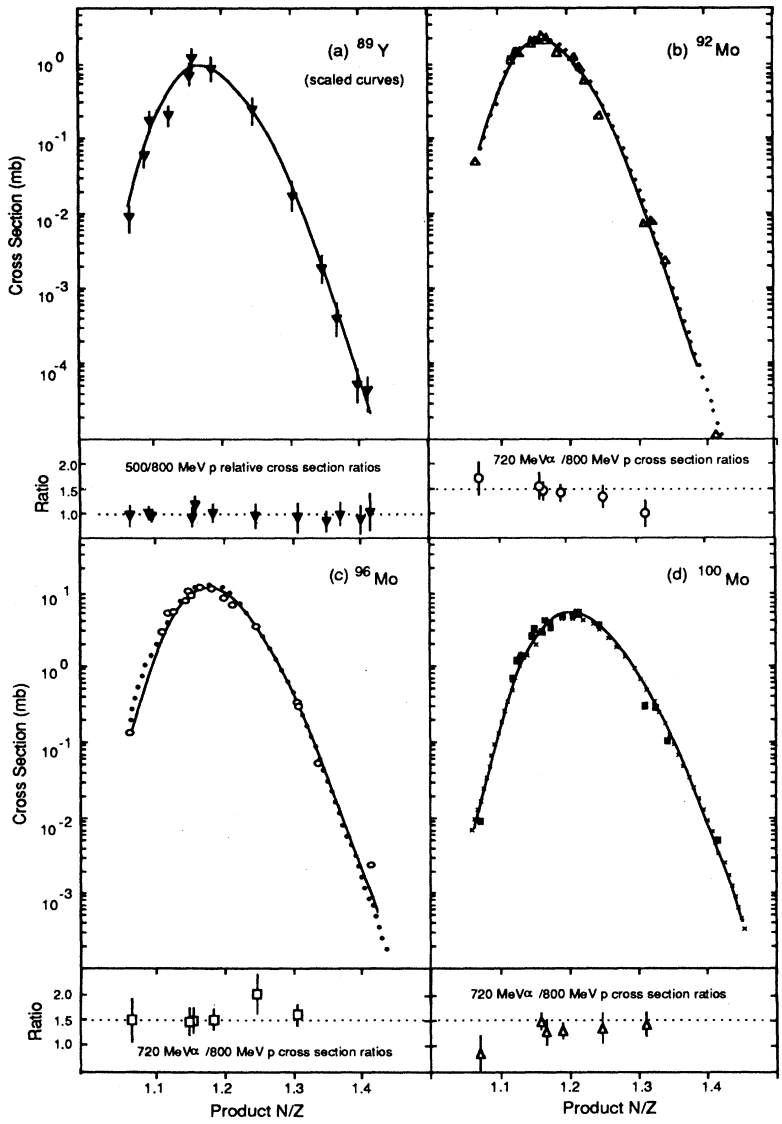

FIG. 2. Comparison of $A=72$ relative isobaric yield curve shapes: (a) 500 MeV protons with 800 MeV protons on ^{89}Y; (b)–(d) 720 MeV alphas with 800 MeV protons for ^{92,96,100}Mo, respectively. Solid curve as in Fig. (1) for 800 MeV protons. Dotted curves through alpha data are fits to Eq. (1).

TABLE V. Fitted shape parameters of $A=72$ isobaric yield curves.

Projectile	μ_1'	$(\mu_2)^{1/2}$	μ_3'	μ_3
^{92}Mo ($N/Z=1.190$)				
800 MeV p	1.159±0.0005	$(4.07\pm0.03)\times10^{-2}$	1.566±0.002	2.04×10^{-5}
720 MeV α	1.162±0.004	$(3.95\pm0.3)\times10^{-2}$	1.575±0.02	1.82×10^{-5}
^{89}Y ($N/Z=1.282$)				
500 MeV p	1.174±0.005	$(4.357\pm0.29)\times10^{-2}$	1.623±0.02	4.13×10^{-5}
800 MeV p	1.176±0.002	$(4.185\pm0.13)\times10^{-2}$	1.632±0.007	3.93×10^{-5}
^{96}Mo ($N/Z=1.286$)				
800 MeV p	1.179±0.0039	$(4.379\pm0.3)\times10^{-2}$	1.649±0.02	4.23×10^{-5}
720 MeV α	1.182±0.0034	$(4.462\pm0.3)\times10^{-2}$	1.657±0.01	3.83×10^{-5}
^{100}Mo ($N/Z=1.381$)				
800 MeV p	1.203±0.0007	$(4.570\pm0.05)\times10^{-2}$	1.747±0.003	3.34×10^{-5}
720 MeV a	1.203±0.003	$(4.718\pm0.2)\times10^{-2}$	1.742±0.01	3.71×10^{-5}
^{130}Te ($N/Z=1.500$)				
800 MeV p	1.227±0.003	$(4.857\pm0.2)\times10^{-2}$	1.854±0.01	-7.79×10^{-6}

cross section of ^{70}As for all targets but ^{130}Te. This observation itself provides a significant clue. Scholz and Malik showed that a short evaporation chain tends to populate high spin states of isomers.[26] Accordingly, the low yield of ^{70}As from the ^{89}Y and $^{92-100}$Mo targets suggests the existence of an unknown short-lived, high-spin, isomeric state that directly feeds the stable ^{70}Ge daughter. Conversely, the much longer evaporation chains required to reach ^{70}As from ^{130}Te present many opportunities for the dissipation of angular momentum,[27] so the ground state predominates. To estimate the ^{70}As^m cross section, we used the observed m/g ratio in Table II of ^{74}Br, a comparable odd-odd, neutron-deficient nuclide whose m/g I_π ratio is $4^-/1^-$. The ^{70}As^{m+g} estimate becomes 6.4 mb, in close agreement with the fitted ^{89}Y isobaric yield curve of Fig. 1(a).

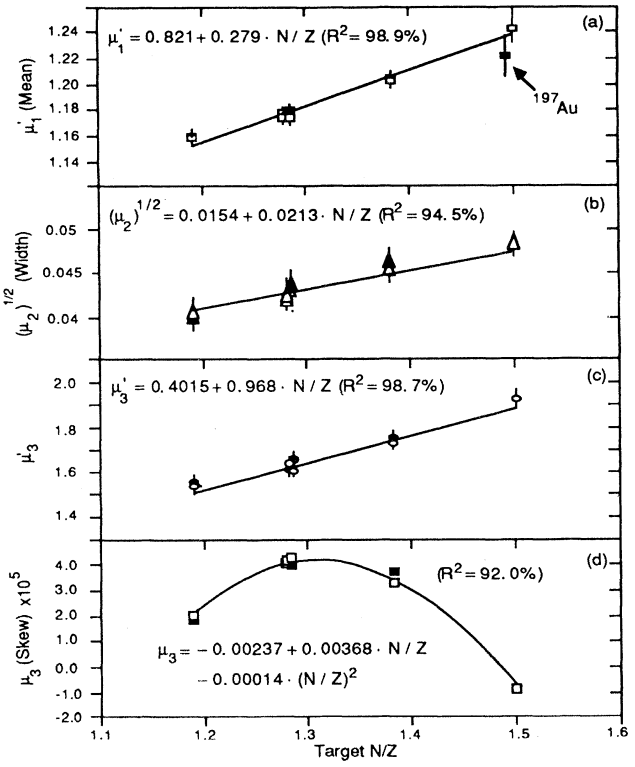

FIG. 3. Variation of isobaric yield curve shape parameters with target N/Z.

Precise knowledge of yield distribution systematics is important for geochemistry, cosmochemistry, and isotope production in the medical and nuclear structure fields. A widely used empirical relationship introduced by Rudstam[28] assumes a symmetric form

$$\sigma(A,Z)=f(A_t,E)\exp\{PA-R[Z-(SA+TA^2)]^\alpha\}\ , \tag{7}$$

where $\sigma(A,Z)$ is the predicted product cross section of nuclide (A,Z), A_t is the target mass number, and E is the projectile energy. The term $(SA+TA^2)$ establishes the position of maximum yield for mass A. α, P, R, S, and T are "best fit" constants to experimental yield, chiefly from the spallation of medium mass targets. P is analogous to the logarithmic mass-yield slope. R is the distribution width parameter. The distribution peak parameters are T and S. With constant S, the peak of the predicted yields distributions does not vary with target N/Z. To account for the marked effect of target composition upon the distribution peak position, Chackett and Chackett[29] and Silberberg and Tsao[30] used more complicated expressions for S.

Calculated isobaric yield curves at $A=72$ for ^{92}Mo and ^{100}Mo targets are compared to the corresponding fitted experimental curves (symbols) in Fig. 4. The Chackett and Chackett (dashed line) and Silberberg and Tsao (solid line) formulations give similar scaled curves in which the experimentally observed shift in peak position with target composition is qualitatively reproduced. Of course, the symmetric functional form of the empirical formulas fails to describe the changing width and asymmetry seen experimentally. Furthermore, although an improvement over Rudstam's pioneering work, errors greater than a factor of 2 are still not uncommon from these modifications.

The regular variation of the shape parameters as a function of target N/Z (Fig. 3) supports their usage in

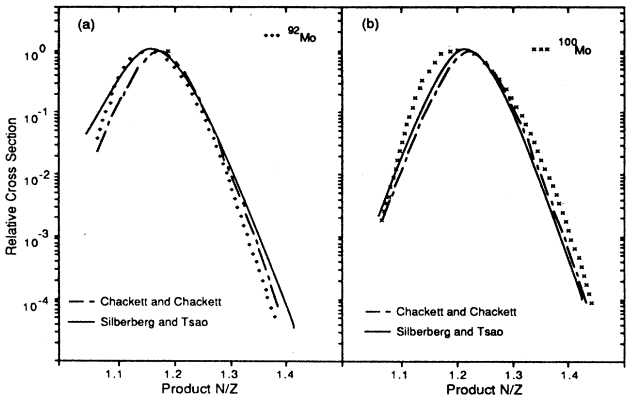

FIG. 4. Comparison of fitted distribution curves from Eq. (1) with empirical formulas for (a) ^{92}Mo and (b) ^{100}Mo targets.

"master curves" to predict the systematic behavior of isobaric yield distributions for all types of incident projectiles. Such trends were, in fact, the premise of Rudstam's original relationship.

V. CONCLUSION

The results of the present study consist of absolute formation yields of products with $65 \leq A \leq 82$ from ^{89}Y, $^{92-100}$Mo and ^{130}Te targets at a proton energy of 800 MeV. Also, relative yields from ^{89}Y using 500 MeV protons were measured. In an attempt to provide a meaningful resolution of the excitation and relaxation steps, particular emphasis was paid to the measurement of product yields away from stability.

By recourse to the established smoothness of spallation systematics, the yields from each target were corrected to conform to $A=72$ isobaric curves. The virtually identical curve shapes at 500 and 800 MeV lends strong support to the argument that the excitation and relaxation stages are not strongly coupled. That argument is further strengthened by the observed dependence of the peak position of the yield distribution upon target composition in spite of the funneling effect of the nuclear energy surface.

Cross sections were used to obtain precise parametrization of spallation yield systematics. The very regular dependence of the mean (peak location), standard deviation (width), and third moment (skewness) of charge dispersion curves on target composition is now well established. In conjunction with a skewed distribution model function, these shape parameters define a set of accurate master relationships useful for predicting the relative yield of spallation products including the ability to reproduce the asymmetric shapes from targets of different composition.

Comparison of the proton-induced yields with those from alpha-induced reactions agree very well with a simple scheme based on total reaction cross section ratios. The observed scaling of proton and alpha-induced yields according to the total reaction cross section is a reflection of factorization.[31] Since total reaction cross sections can be calculated for hadronic projectiles over an extensive energy domain with the soft spheres model, spallation systematics can be extrapolated with reasonable confidence over a wide domain.[32,33] However, spallation systematics are not justifiable when other reaction mechanisms like multifragmentation,[2] fission,[34] and electromagnetic dissociation[35] become appreciable.

ACKNOWLEDGMENTS

This study was sponsored by the U. S. Department of Energy. The authors wish to acknowledge the hospitality and assistance of Dr. B. J. Dropesky, Dr. L. C. Liu, and Dr. G. C. Giesler of Los Alamos National Laboratory. One of us (M.J.T.) submitted this work in partial fulfillment for the Ph.D. degree, Department of Chemistry, Carnegie-Mellon University.

[1] R. Serber, Phys. Rev. **72**, 1114 (1947).
[2] J. Hüfner, Phys. Rep. **125** 129 (1985).
[3] W. G. Lynch, Annu. Rev. Nucl. Part. Sci. **37**, 493 (1987).
[4] B. S. P. Shen and M. Merker, *Spallation Nuclear Reactions and their Applications* (Reidel, Dordrecht, 1976), Vol. 59.
[5] J. A. Miskel, M. L. Perlman, G. Friedlander, and J. M. Miller, Phys. Rev. **98**, A1197 (1955).
[6] G. Rudstam, E. Bruninx, and A. C. Pappas, Phys. Rev. **126**, 1852 (1962).
[7] J. M. Miller and J. Hudis, Annu. Rev. Nucl. Sci. **9**, 159 (1959).
[8] I. Dostrovsky, P. Rabinowitz, and R. Bivins, Phys. Rev. **11**, 1659 (1958).
[9] N. T. Porile and L. B. Church, Phys. Rev. **133**, B310 (1964).
[10] C. Thibault-Philippe, Doctoral dissertation, University of Paris, 1971 (unpublished).
[11] T. H. Ku and P. J. Karol, Phys. Rev. C **16**, 1984 (1977).
[12] M. J. Tobin and P. J. Karol, Phys. Rev. C **38**, 267 (1988).
[13] E. F. Norton, *Chemical Yield Determinations in Radiochemistry,* Nuclear Science Series NAS-NA-311 (National Academy of Science—National Research Council, Washington D. C., 1970).
[14] C. M. Lederer and V. S. Shirley, *Table of Isotopes,* 7th ed. (Wiley, New York 1978).
[15] U. Reus and W. Westmeier, At. Data Nucl. Data Tables, **29**, 193 (1983).
[16] J. B. Cumming, in *Application of Computers to Nuclear and Radiochemistry,* Nuclear Science Series NAS-NS-3107, edited by G. D. O'Kelley (National Academy of Sciences—National Research Council, Washington D. C., 1963).
[17] J. B. Cumming, Annu. Rev. Nucl. Sci. **13**, 261 (1963).
[18] P. J. Karol, Phys. Rev. C **10**, 150 (1974).
[19] S. Kaufman, Phys. Rev. **129**, 1866 (1963).
[20] J. B. Cumming, P. E. Haustein, T. J. Ruth, and G. J. Virtes, Phys. Rev. C **17**, 1632 (1978).
[21] P. J. Karol, Department of Energy Report No. DOE-4721-5, 1981 (unpublished).
[22] M. Abramowitz and I. A. Stegun, *Handbook of Mathematical Functions* (Dover, New York, 1970).
[23] P. J. Karol, M. J. Tobin, and S. Shibata, Phys. Rev. C **28**, 1850 (1983).

[24]K. LeCouteur, Proc. Phys. Soc. London **A63**, 259 (1950); **A65**, 718 (1952).
[25]P. J. Karol, Phys. Rev. C **11**, 1203 (1975).
[26]W. Scholz and F. B. Malik, Phys. Rev. **176**, 1355 (1968).
[27]G. Rudstam, Phys. Scr. **20**, 165 (1979).
[28]G. Rudstam, Z. Naturforsch. **21a**, 1027 (1966).
[29]K. F. Chackett and G. A. Chackett, Nucl. Phys. **A100**, 633 (1967).
[30]R. Silberberg and C. H. Tsao, Astrophys. J. Suppl. Ser. **25**, 313 (1973); **25**, 335 (1973).
[31]A general discussion of factorization is presented in H. Boggild and T. Ferbel, Annu. Rev. Nucl. Sci. **24**, 451 (1974).
[32]S. Kox, A. Gamp, C. Perrin, J. Arvieux, R. Bertholet, J. F. Bruandet, M. Buenerd, R. Cherkaoui, A. J. Cole, Y. El-Masri, N. Longequeue, J. Menet, F. Merchez, and J. B. Viano, Phys. Rev. C **35**, 1678 (1987).
[33]P. J. Karol, Astrophys. J. **332**, 615 (1988).
[34]Y. Y. Chu, E. M. Franz, G. Friedlander, and P. J. Karol, Phys. Rev. C **4**, 2202 (1971).
[35]J. C. Hill, J. A. Winger, C. M. McCullough, A. R. Smith, J. B. McCaslin, and P. J. Karol, Phys. Rev. C **33**, 557 (1986).